Anharmonic effects in the phonon spectra of sodium chloride

E. R. Cowley
Physics Department, Brock University, St. Catherines, Ontario L2S 3A1, Canada

G. Jacucci*
Centre Européen de Calcul Atomique et Moléculaire, Faculté des Sciences, 91405 Orsay, France

M. L. Klein†
Laboratoire de Physique Théorique des Liquides, Université Pierre et Marie Curie, 75230 Paris, France

I. R. McDonald
Chemistry Department, Royal Holloway College, Egham, Surrey TW20 0EX, England
(Received 9 February 1976)

Results are reported of a series of molecular-dynamics "experiments" on solid NaCl at temperatures of 80, 302, 954, and 1153 K. Attention is focused primarily on the computation of the dynamical structure factor and its one-phonon approximation; comparison of the two allows the isolation of contributions from multiphonon and interference terms. Anharmonic effects are analyzed in terms of perturbation theory and the theory is found to give satisfactory results for the phonon frequencies at temperatures up to 80% that of melting. Most of the calculations are carried out for a simple rigid-ion potential, but the effects of polarization and its incorporation in molecular-dynamics calculations are briefly discussed.

I. INTRODUCTION

The lattice vibrations of NaCl, the protype ionic crystal, were first analyzed in detail in the classic paper of Kellermann.[1] Kellermann's calculations were based on the assumption that the crystal is composed of rigid ions interacting through a potential in which a short-range repulsion is superimposed on the long-range Coulombic term. This simple model, even in the more elaborate version of Tosi and Fumi,[2] is unable to account quantitatively for the dynamical properties of NaCl, as revealed by neutron spectroscopy,[3] because it neglects the effects of ionic polarization. Several models exist which remedy this defect,[4-6] and one of these (the shell model of Dick and Overhauser[4]) is discussed briefly in Sec. IV F. However, the motivation for the work presented here lies in the question of the general nature of the lattice vibrations in NaCl-type crystals at high temperatures and their interpretation in terms of anharmonic perturbation theory. For that reason we have carried out most of our calculations with the Tosi-Fumi rigid-ion potential, a model which is known to give a good fit to many equilibrium crystal properties.[7]

The melting point of NaCl at atmospheric pressure is 1073 K, or approximately three times its Debye temperature. Above room temperature it may be treated as essentially a classical solid and classical theories of anharmonic lattice dynamics[8] may therefore be applied. Such methods have indeed been used successfully in the interpretation of thermodynamic[9] and optical data[10] on NaCl. However, there exist few direct data on the phonons at elevated temperatures (above two-thirds that of melting), where a breakdown of simple perturbation approaches to the problem of vibrational anharmonicity[11] can be expected. To make it possible to study anharmonic effects in the range of temperature in which experimental data are lacking, we have carried out a series of computer simulations by the method of molecular dynamics, the primary purpose being the calculation of the dynamic structure factor $S(\vec{Q}, \omega)$. The latter, as is well known, is related in a simple way to the double differential cross section for coherently scattered thermal neutrons, whereas the intensity of x-ray scattering is related to the integral of $S(\vec{Q}, \omega)$ over all ω. The basis of the molecular-dynamics method is the solution of Newton's equations of motion for a finite system of particles contained in a box with periodic boundary conditions. From the classical phase-space trajectories which this procedure yields, ensemble averages of the type encountered in statistical mechanics are readily evaluated. The outstanding virtue of the method is that it yields results which are essentially exact *for the system studied*. This means, in the present case, that the predictions of perturbation theory can be tested in an unambiguous way if carried out for the same model. We wish to emphasize at the outset that our definition of the model includes the fact that a small periodic system is used. In particular, the lattice-dynamical calculations have been made over a mesh of points in the Brillouin zone which is consistent with the size of the molecular-dynamics system.

The computer "experiments" yield with equal ease both the full multiphonon $S(\vec{Q}, \omega)$ and its one-phonon approximation $S_1(\vec{Q}, \omega)$. This makes it possible to investigate the convergence of the standard phonon expansion of $S(\vec{Q}, \omega)$. Moreover, a study of the $\vec{Q}$ dependence of various phonons can be expected to reveal the interesting interference effects of the type first identified in the beautiful work of Cowley and Buyers[12] and also discussed in an important paper by Horner.[13]

Four separate molecular-dynamics runs have been carried out. The first, for a temperature of 80 K, was designed to test the accuracy of the simulation by comparison with the results of quasiharmonic lattice dynamics for the same interionic potential. The second, at 302 K, was made in order to compare with calculations based on anharmonic perturbation theory in a range of temperature where the theory should work well. The other two "experiments," at 954 and 1153 K, were carried out specifically to probe possible inadequacies in the perturbation theory of anharmonic effects in the region where these effects are largest. Anticipating some of our conclusions, we shall see in Sec. IV E that the perturbation results are surprisingly good, but that important differences in detail remain. We shall also see that all the interesting manifestations of vibrational anharmonicity are contained in our results. The method, of course, can easily be used in the study of other alkali halides.

II. MOLECULAR-DYNAMICS CALCULATIONS

The molecular-dynamics calculations were carried out on a system of 216 particles, consisting of 108 positive (Na^+) and 108 negative (Cl^-) ions disposed on the interpenetrating fcc lattices of the NaCl crystal structure and lying within a cubic cell of length L. Periodic boundary conditions were imposed and the classical equations of motion of the ions were solved by means of a simple finite difference algorithm,[14] with a time step in the numerical integrations of 7×10^{-15} sec. The interionic pair potential used was the generalized Huggins-Mayer potential with parameters deduced from solid-state thermodynamic data by Tosi and Fumi,[2] namely

$$\phi_{ij}(r_{ij}) = z_i z_j/r_{ij} + c_{ij} b \exp[(\sigma_i + \sigma_j - r_{ij})/\rho] - C_{ij}/r_{ij}^6 - D_{ij}/r_{ij}^8 , \quad (1)$$

where z_i and z_j are the charges on ions labeled i and j, located at $\vec{r}_i, \vec{r}_j$ and separated by a distance $r_{ij} = |\vec{r}_i - \vec{r}_j|$. The second term on the right-hand side of Eq. (1) describes the overlap repulsion between ions. In this term the factor b takes the same value for all alkali halides which crystallize in the NaCl-type structure, σ_i and σ_j are lengths ("basic radii") characteristic of the ions, ρ is a "hardness parameter" characteristic of the particular salt, and the c_{ij} are numerical constants introduced by Pauling. The last two terms in Eq. (1) represent the contributions, respectively, from dipole-dipole and dipole-quadrupole dispersion forces. As we have already remarked, the major weakness of the Tosi-Fumi model, at least insofar as the calculation of lattice vibrations is concerned, is the fact that no explicit account is taken of the effects of ionic polarization. We shall return briefly to this question in Sec. IV F. Values of the potential parameters used in the calculations are listed in Table I and details of the thermodynamic states which were studied are summarized in Table II. In Table II we also give the total number of time steps which were generated at each state point.

TABLE I. Parameters in the Tosi-Fumi potential for NaCl.

b	3.38×10^{-13} erg
c_{++}	1.25
c_{+-}	1
c_{--}	0.75
σ_+	1.170 Å
σ_-	1.585 Å
ρ	0.317 Å
C_{++}	1.68×10^{-60} erg cm^6
C_{+-}	11.2×10^{-60} erg cm^6
C_{--}	116×10^{-60} erg cm^6
D_{++}	0.8×10^{-76} erg cm^8
D_{+-}	13.9×10^{-76} erg cm^8
D_{--}	233×10^{-76} erg cm^8

Use of a periodic boundary condition makes it possible to employ the Ewald method for the calculation of the electrostatic energy. In doing so we have exploited an idea due to Singer (private communication) whereby the total electrostatic energy E_C is written in the exact form given by

$$E_C = \tfrac{1}{2}\sum_{n\neq 0} A_n(\eta)(C_{\vec{n}}^2 + S_{\vec{n}}^2) + \sum_i z_i \sum_{j>i} z_j \frac{\mathrm{erfc}(\eta r_{ij})}{r_{ij}} - \sum_i \frac{z_i^2 \eta}{\pi^{1/2}} . \quad (2)$$

The symbol erfc is used to denote the complementary error function, $\mathrm{erfc}(x) = 1 - \mathrm{erf}(x)$, and

$$A_n(\eta) = \frac{\exp(-\pi^2 n^2/\eta^2 L^2)}{n^2} , \quad (3)$$

$$C_{\vec{n}} \equiv \sum_i c_{\vec{n}i} = \sum_i z_i \cos\left(2\pi \frac{\vec{n}\cdot\vec{r}_i}{L}\right) , \quad (4)$$

TABLE II. Selected equilibrium properties of NaCl.

Source	T (K)	V ($cm^3\,mol^{-1}$)	pV/NkT	$-U$ ($kJ\,mol^{-1}$)	$\langle u_+^2\rangle^{1/2}$ (Å)	$\langle u_-^2\rangle^{1/2}$ (Å)	Time steps (1000's)
MD [a]	80.3	26.92	0.08	773.5	0.126	0.113	10
Expt. [b]	298.0	27.0	0.0	764.0			
MC [c]	298.0	27.65	0.0	762.6			
MD	301.7	27.60	0.13	762.1	0.234	0.227	6
MD	953.8	29.50	0.87	727.3	0.494	0.460	10
Expt.	1073.0	30.0	0.0	719.6			
MC	1073.0	31.37	0.0	717.4			
MD	1153.0	31.37	0.21	713.2	0.611	0.577	28.8

[a] MD, results from present molecular-dynamics calculations.
[b] Expt., experimental data (Ref. 7).
[c] MC, results from Monte Carlo calculations (Ref. 7).

$$S_{\vec{n}} \equiv \sum_i s_{\vec{n}i} = \sum_i z_i \sin\left(2\pi \frac{\vec{n}\cdot\vec{r}_i}{L}\right) . \tag{5}$$

The quantity η is a disposable parameter (having dimensions length^{-1}) which governs the relative rate of convergence of the two series in Eq. (2), one of which is an expansion in reciprocal space, the other being a sum in real space. The first term on the right-hand side of Eq. (2) involves a summation over reciprocal-lattice vectors n of the simple cubic structure of cells of side L, together with a sum over particles within one such cell. The advantage of writing the reciprocal-space term in the particular form quoted here is that the summation over ions runs only over *single* ions rather that pairs, with a correspondingly large reduction in the length of the computations. The real-space summation in Eq. (2) is taken over pairs i,j within a single cell. Finally, differentiation of E_C with respect to the coordinates of ion i yields the Coulombic force $\vec{F}_{Ci}$ on ion i as

$$\vec{F}_{Ci} = -\sum_{n\neq 0} \vec{n}\left(\frac{2\pi}{L}\right) A_n(\eta)(c_{\vec{n}i}S_{\vec{n}} - s_{\vec{n}i}C_{\vec{n}}) + z_i \sum_{j\neq i} \vec{r}_{ij} z_j \left(\frac{\operatorname{erfc}(\eta r_{ij})}{r_{ij}^3} + \frac{2\eta}{\pi^{1/2}} \frac{\exp(-\eta r_{ij}^2)}{r_{ij}^2}\right) . \tag{6}$$

Equation (6) has been used in all our molecular dynamics calculations. The parameter η was taken as $5.6/L$ and the reciprocal-space term was evaluated for 309 pairs of vectors, account being taken of the fact that vectors $\vec{n}$ and $-\vec{n}$ make identical contributions both to E_C and to $\vec{F}_{Ci}$. The real-space term was truncated at $r_{ij} = \frac{1}{2}L$, the same cutoff in the potential being used for the non-Coulombic terms in (1).

Our main effort has been directed at the calculation of the dynamical structure factor $S(\vec{Q},\omega)$, which we have computed in the manner of Levesque, Verlet, and Kürkijarvi[14] from the classical expression

$$S(\vec{Q},\omega) = \frac{1}{N}\int_0^\infty e^{i\omega t}\langle \rho_{\vec{Q}}(t)\rho_{-\vec{Q}}(0)\rangle\, dt = \lim_{\tau\to\infty}\frac{1}{N\tau}\int_0^\tau e^{-i\omega t}\rho_{\vec{Q}}(t)\,dt \int_0^\tau e^{i\omega t'}\rho_{-\vec{Q}}(t')\,dt' = \frac{1}{N}\lim_{\tau\to\infty}\frac{1}{\tau}\,|\rho_{\vec{Q}}(\omega)|^2 , \tag{7}$$

where N is the number of ions of each type (i.e., the number of unit cells), $\hbar\vec{Q}$ is the momentum transfer, $\hbar\omega$ is the energy transfer, and $\rho_{\vec{Q}}(\omega)$ is the Fourier-Laplace transform of the particle density $\rho_{\vec{Q}}(t)$. The latter we write in terms of partial densities as

$$\rho_{\vec{Q}}(t) = \rho^+_{\vec{Q}}(t) + \rho^-_{\vec{Q}}(t) , \tag{8}$$

with

$$\rho^+_{\vec{Q}}(t) = \sum_{\text{cations}} e^{i\vec{Q}\cdot\vec{r}_i(t)} , \qquad \rho^-_{\vec{Q}}(t) = \sum_{\text{anions}} e^{i\vec{Q}\cdot\vec{r}_j(t)} . \tag{9}$$

Thus the calculation of $S(\vec{Q},\omega)$ reduces to the calculation of partial dynamical structure factors $S_{\alpha\beta}(\vec{Q},\omega)$, i.e., the Fourier transforms of correlation functions $\langle \rho^\alpha_{\vec{Q}}(t)\rho^\beta_{-\vec{Q}}(0)\rangle$, where $\alpha,\beta = +,-$ and $S_{+-}(\vec{Q},\omega) = S_{-+}(\vec{Q},\omega)$. Specifically,

$$S(\vec{Q},\omega) = S_{++}(\vec{Q},\omega) + S_{--}(\vec{Q},\omega) + 2S_{+-}(\vec{Q},\omega) . \tag{10}$$

On the other hand, the cross section for the coherent inelastic scattering of neutrons, $S^n(\vec{Q},\omega)$, is constructed by weighting the partial quantities occurring in Eq. (10) by neutron scattering lengths. The x-ray scattering intensity would be obtained by weighting with the appropriate form factors and integrating over ω. Similarly, the spectrum of charge density fluctuations, representing the optic modes of vibrations, is obtained by weighting with the charges of the ions. Thus

$$S^n(\vec{Q},\omega) = b_+^2 S_{++}(\vec{Q},\omega) + b_-^2 S_{--}(\vec{Q},\omega) + 2b_+ b_- S_{+-}(\vec{Q},\omega) \tag{11}$$

and

$$S^z(\vec{Q},\omega) = z_+^2 S_{++}(\vec{Q},\omega) + z_-^2 S_{--}(\vec{Q},\omega) + 2z_+ z_- S_{+-}(\vec{Q},\omega) . \tag{12}$$

The phonon frequencies measured in a neutron experiment can be identified with the peaks in $S^n(\vec{Q},\omega)$, in the calculation of which we have used the reduced scattering lengths $b_+ = 0.52$ and $b_- = 1.47$.

During the course of the molecular-dynamics runs we also evaluated the one-phonon approximation to $S(\vec{Q},\omega)$, denoted by $S_1(\vec{Q},\omega)$, which may be computed in the same way as $S(\vec{Q},\omega)$ itself except that $\rho_{\vec{Q}}(t)$ in Eq. (7) is replaced by $\tilde{\rho}_{\vec{Q}}(t)$, defined as

$$\tilde{\rho}_{\vec{Q}}(t) = \tilde{\rho}^+_{\vec{Q}}(t) + \tilde{\rho}^-_{\vec{Q}}(t) , \tag{13}$$

where, for example,

$$\tilde{\rho}^+_{\vec{Q}}(t) = d_+(Q) \sum_{\text{cations}} e^{i\vec{Q}\cdot\vec{R}_i} \vec{Q}\cdot\vec{u}_i(t) . \tag{14}$$

The quantity $d_+(Q)$ is related to the Debye-Waller factor (see Sec. III below) and

$$\vec{u}_i(t) = \vec{r}_i(t) - \vec{R}_i \tag{15}$$

is the instantaneous displacement of the ith ion from its lattice site $\vec{R}_i$. The one-phonon approximations to $S^n(\vec{Q},\omega)$ [i.e., $S_1^n(\vec{Q},\omega)$] and $S^z(\vec{Q},\omega)$ [i.e., $S_1^z(\vec{Q},\omega)$] are constructed in an analogous way, account being taken of the different weighting of the partial structure factors.

The length of the molecular dynamics cell (for $N = 108$) is $L = 3a$, where a is the lattice constant, i.e., twice the separation d of neighboring Na^+ and Cl^- lattice sites. From the periodic nature of the system it follows that the *independent* values of momentum transfer which we can study are limited to $\vec{Q} = (2\pi/3a)(n_1, n_2, n_3)$, where the n_i are integers. For example, in the $\langle 100\rangle$ direction, we are limited to studying three different values of the phonon wave vector $\vec{q}$. However, we can study the same "phonon" for several different values of the momentum transfer because we can always write $\vec{q} = \vec{Q} \pm \vec{g}$, where $\vec{g}$ is any Bragg vector. It should also be noted that the appearance of terms of the form $\vec{Q}\cdot\vec{u}$ in both (9) and (14) means that we cannot study transverse phonons in the first Brillouin zone, a limitation which applies with equal force in a real neutron scattering experiment.

Finally, we note that our computations must satisfy the Placzek sum rule

$$\frac{1}{2\pi}\int_0^\infty \omega^2 S(\vec{Q},\omega)\, d\omega = \tfrac{1}{2} kTQ^2\left(\frac{1}{m_+} + \frac{1}{m_-}\right), \tag{16}$$

where m_+, m_- are the ionic masses. This provides a useful check on the accuracy of the molecular-dynamics results. In practice the rule is satisfied to within a few percent, except at the lowest temperature. There, because the peak in $S(\vec{Q},\omega)$ is very sharp, the fact that the spectrum is sampled only at discrete values of ω can cause the second moment to be considerably in error.

III. LATTICE DYNAMICS

In this section we briefly indicate the relationship of usual phonon calculations[8-10] to the computer simulation work reported here. Our starting point is an expression for the time correlation function occurring in Eq. (7), i.e.,

$$S(\vec{Q},t) \equiv \frac{1}{N}\langle \rho_{\vec{Q}}(t)\rho_{-\vec{Q}}(0)\rangle = \frac{1}{N}\sum_{i,j} e^{X_{ij}}\langle e^{x_i} e^{y_j}\rangle , \tag{17}$$

where $X_{ij} = i\vec{Q}\cdot(\vec{R}_i - \vec{R}_j)$, $x_i = i\vec{Q}\cdot\vec{u}_i(t)$, and $y_j = -i\vec{Q}\cdot\vec{u}_j(0)$. The labels $i \equiv l, \kappa$ and $j \equiv l, \kappa'$ are used to denote the κth (or κ'th) ion in the lth (or l'th) unit cell; thus $\vec{u}_i(t)$ denoted the displacement of the κth ion in the lth unit cell from its equilibrium position $\vec{R}_i$.

Ambegoakar, Conway, and Baym[15] have shown that from an expression of the type of (17) a Debye-Waller factor can be rigorously separated out. In the classical case we may write

$$\langle e^{x_i} e^{y_j}\rangle = d(x_i)d(y_j)\left[1 + \langle x_i y_j\rangle + \tfrac{1}{2}(\langle x_i^2 y_j\rangle - \langle x_i y_j^2\rangle) + \tfrac{1}{2}\langle x_i y_j\rangle^2 + \cdots\right] . \tag{18}$$

Successive terms on the right-hand side of this equation are the correlation functions corresponding to elastic, one-phonon, lowest-order interference, and lowest-order two-phonon contributions to $S(\vec{Q},t)$. The Debye-Waller factor $d(x_i)$ is defined in terms of a cumulant expansion as

$$\ln d(x_i) = (1/2!)\langle x_i^2\rangle + (1/4!)(\langle x_i^4\rangle - 3\langle x_i^2\rangle^2) + \cdots . \tag{19}$$

For a cubic crystal, Eq. (19) can be written in a more transparent notation as $d(x_i) \equiv d_\kappa(Q)$, with

$$d_\kappa(Q) \simeq \exp(-\tfrac{1}{6} Q^2\langle u_\kappa^2\rangle) . \tag{20}$$

The one-phonon approximation for $S(\vec{Q},t)$ follows immediately. On substituting (18) into (17) we find that

$$S_1(\vec{Q},t) = \frac{1}{N}\langle \tilde{\rho}_{\vec{Q}}(t)\tilde{\rho}_{-\vec{Q}}(0)\rangle , \tag{21}$$

where $\tilde{\rho}_{\vec{Q}}(t)$ is the density operator defined by (13). We now introduce the quantities $\hat{\rho}^+_{\vec{Q}}(t)$ and $\hat{\rho}^-_{\vec{Q}}(t)$ where, for example,

$$\hat{\rho}^{+}_{\vec{Q}}(t) = \sum_{\text{cations}} e^{i\vec{Q}\cdot\vec{R}_i}\vec{\xi}\cdot\vec{u}_i(t)\,, \tag{22}$$

with $\vec{Q} = Q\vec{\xi}$. With the aid of (22) we can rewrite Eq. (21) in the form

$$\begin{aligned}(N/Q^2)S_1(Q,t) &= d_+^2(Q)\langle\hat{\rho}^{+}_{\vec{Q}}(t)\hat{\rho}^{+}_{-\vec{Q}}(0)\rangle \\ &\quad + d_-^2(Q)\langle\hat{\rho}^{-}_{\vec{Q}}(t)\hat{\rho}^{-}_{-\vec{Q}}(0)\rangle \\ &\quad + 2d_+(Q)d_-(Q)\langle\hat{\rho}^{+}_{\vec{Q}}(t)\hat{\rho}^{-}_{-\vec{Q}}(0)\rangle \\ &\equiv [Qd(Q)]^2F\,,\end{aligned} \tag{23}$$

which serves as a formal definition of the quantity $d(Q)$; F is a correlation function which is independent of Q.

To proceed further in lattice-dynamical calculations it is necessary to evaluate the correlation function $\langle\vec{u}_i(t)\cdot\vec{u}_j(0)\rangle$. This is done by introducing normal coordinates derived from the eigenfrequencies $\omega_{\vec{q}\lambda}$, i.e., the harmonic frequencies of wave vector $\vec{q}$ and polarization λ, and their associated eigenvectors $\vec{e}^{\kappa}_{\vec{q}\lambda}$. In the harmonic approximation (and the classical limit) the result is

$$S_1(\vec{Q},\omega) = \frac{kT}{\omega}\sum_{\lambda}\Delta(\vec{Q}-\vec{q})\,|F_{\vec{q}\lambda}(\vec{Q})|^2A^0_{\vec{q}}(\omega)\,, \tag{24}$$

where $\Delta(\vec{Q}-\vec{q})$ is the crystal δ function, the spectral function $A^0_{\vec{q}\lambda}(\omega)$ is given by

$$A^0_{\vec{q}\lambda}(\omega) = 2\pi[\delta(\omega-\omega_{\vec{q}\lambda}) - \delta(\omega+\omega_{\vec{q}\lambda})]\,, \tag{25}$$

and the one-phonon inelastic structure factor $F_{\vec{q}\lambda}(\vec{Q})$ is defined as

$$F_{\vec{q}\lambda}(\vec{Q}) = \sum_{\kappa} d_\kappa(Q)\,e^{i\vec{q}\cdot\vec{R}_\kappa}(i\vec{Q}\cdot\vec{e}^{\kappa}_{\vec{q}\lambda})/(2m_\kappa\omega_{\vec{q}\lambda})^{1/2} \tag{26}$$

Thus the spectrum is given as a sum of δ-function peaks of appropriate weights.

For an anharmonic crystal the problem is more difficult, requiring the use of many-body perturbation theory.[8-10] However, the results bear a strong similarity to those for a harmonic crystal, provided that the coupling of one-phonon states corresponding to the same wave vector but different polarization branches is neglected. This so-called polarization mixing effect vanishes for the zone-center modes, and elsewhere is usually assumed to be small. The expression for $S_1(\vec{Q},\omega)$ is then the same as that obtained in the harmonic case, except that the δ functions are broadened and shifted by the phonon-phonon interactions. The effect is to replace the spectral function (25) by

$$A_{\vec{q}\lambda}(\omega) = \frac{8\omega^2_{\vec{q}\lambda}\Gamma_{\vec{q}\lambda}(\omega)}{[-\omega^2+\omega^2_{\vec{q}\lambda}+2\omega_{\vec{q}\lambda}\Delta_{\vec{q}\lambda}(\omega)]^2+[2\omega_{\vec{q}\lambda}\Gamma_{\vec{q}\lambda}(\omega)]^2}\,. \tag{27}$$

$\Delta_{\vec{q}\lambda}(\omega)$ and $\Gamma_{\vec{q}\lambda}(\omega)$ are related to the anharmonic terms in the Taylor series expansion of the total potential energy of the crystal in powers of the displacements of the ions from their equilibrium positions.[8] To second order in the cubic anharmonicity and first order in the quartic anharmonicity the shift is given by

$$\begin{aligned}\Delta_1(\omega) &= 12kT\sum_2\frac{V(1,-1,2,-2)}{\omega_2} \\ &\quad - 18kT\sum_{2,3}|V(1,2,3)|^2\left(\frac{(\omega_1+\omega_2)^2}{(\omega_1+\omega_2)^2-\omega^2}\right) \\ &\quad\times\left(\frac{2}{\omega_1\omega_2}\right)\end{aligned} \tag{28}$$

and the width by

$$\begin{aligned}\Gamma_1(\omega) &= 18kT\sum_{2,3}|V(1,2,3)|^2\left(\frac{\omega_1+\omega_2}{\omega_1\omega_2}\right) \\ &\quad\times\pi[\delta(\omega_1+\omega_2-\omega)-\delta(\omega_1+\omega_2+\omega)]\,,\end{aligned} \tag{29}$$

where $\omega_1 \equiv \omega_{\vec{q}_1\lambda_1}$, etc., and the matrix elements V are essentially the Fourier transforms of the cubic and quartic terms in the potential energy.

In the case where polarization mixing is included, the Green's functions are obtained as a matrix with finite nondiagonal terms. The one-phonon contributions to $S(\vec{Q},\omega)$ can be expressed as a sum over all the elements multiplied by appropriate products of structure factors. The detailed formalism has been given by Cowley.[8]

In the actual lattice-dynamical calculations reported here, the $\omega_{\vec{q}\lambda}$ and $\vec{e}^{\kappa}_{\vec{q}\lambda}$ were calculated from the interionic potential (1) for lattice spacings identical to those used in the simulations. This is the so-called quasiharmonic (QH) approximation, use of which allows the harmonic frequencies to change with volume. Similarly, the anharmonic force constants V in (28) and (29) were evaluated for each volume. Coulomb contributions to the harmonic and cubic terms were evaluated using an Ewald transformation. All other types of force, and the Coulomb contribution to the quartic shifts, were summed in real space over enough shells of neighbors to give a converged result.

The principal parts and δ functions appearing in expressions (28) and (29) were replaced by analytic functions corresponding to a finite width. In the usual applications[10] of this technique the expectation is that when a sufficiently fine mesh of wave vectors is used the results become independent of the width of the function used. In the present case the number of wave vectors is fixed at 108. We must then of necessity use quite a wide representation of the δ function. In fact the value used in all of the present calculations corresponds

to a full width at half-maximum of 0.3×10^{13} sec^{-1}. The most obvious justification for such a smoothing function is that the intermediate phonons themselves have finite lifetimes, so that the necessary width can be estimated from a suitable average lifetime. The value we have used then corresponds quite well to what we should estimate for 300 K. For higher temperatures the phonons are less well defined and we can expect that the response functions may show even less structure than we have calculated. For lower temperatures, however, the use of a mesh of the size together with a reasonable estimate of the phonon widths leads to the response functions having a spiky appearance. This may possibly indicate that at the lowest temperatures (i.e., below 300 K) the size of sample we have used cannot be considered "large," but at the higher temperatures it should be satisfactory.

We have calculated the scattering function both with and without the inclusion of the polarization mixing terms. For the particular examples shown here the effect is not large, but we hope to consider other examples in later work. We whall refer to calculations based on Eqs. (27)–(29) as anharmonic perturbation theory (APT).

We wish to stress that our definition of the one-phonon approximation ensures that $S_1(\vec{Q}, \omega)/[Qd(Q)]^2$ is independent of Q. Hence a study of the quantity $S(\vec{Q}, \omega)/[Qd(Q)]^2$ provides a simple means of monitoring the effects of higher-order terms in the phonon expansion (18), i.e., effects due to interference and multiphonon processes.

IV. MOLECULAR-DYNAMICS RESULTS

A. Equilibrium properties

Results on selected equilibrium properties (pressure, internal energy and rms displacements) are shown in Table II. In the case of thermodynamics properties there is fair agreement with previous Monte Carlo calculations[7] based on the same potential model, and also with experimental measurements. The highest temperature studied is actually above the melting point (at atmospheric pressure) of real NaCl. In the simulation, however, the crystal is apparently still stable. In particular, the pressure is positive and the quasiharmonic normal-mode frequencies are all real. The rms amplitude of vibration of the ions is very large at high temperatures, but is everywhere in fair agreement with the results of quasiharmonic lattice-dynamical calculations. It is evident from these results that anharmonicity makes only a small contribution to the mean-square displacement of the ions. However, the molecular-dynamics results, which contain all anharmonic effects, are systematically larger than those obtained from the quasiharmonic calculations. In the harmonic approximation the mean-square displacement is given by

$$\langle u_\kappa^2\rangle = \frac{kT}{Nm_\kappa}\sum_{\vec{q}\lambda}\left(\frac{|\vec{e}_{\vec{q}\lambda}^{\,\kappa}|}{\omega_{\vec{q}\lambda}}\right)^2 . \tag{30}$$

The dominant contribution to this expression comes from the lowest frequency branch of the dispersion curve, i.e., the TA mode. In this branch the anharmonic frequency shift is negative, as we shall see below. Thus the effect of anharmonicity is to increase the mean-square displacement.

B. Temperature dependence of the phonons

In all four molecular-dynamics runs, $S(\vec{Q}, \omega)$ was calculated for the following values of the wave vector $\vec{Q}$ (expressed in units of $2\pi/3a$):

(1, 0, 0), (1, 1, 0), (1, 1, 1), (2, 0, 0),

(2, 2, 0), (3, 0, 0), (3, 3, 0), (0, 2, 4),

(0, 1, 5), (3, 3, 3), (0, 6, 1), (0, 6, 2),

(0, 6, 3), (7, 0, 0), (9, 9, 9), (10, 10, 10).

Additionally, at 302 and 954 K, we studied the points (2, 2, 2), (4, 4, 4), and (8, 8, 8), while at 80 and 1153 K we studied also the points (4, 2, 2), and (6, 0, 0).

Figure 1 shows the calculated phonon frequencies along the ⟨100⟩ direction at 80 K. For each of the four modes, the molecular dynamics results agree well with those of quasiharmonic theory. On the other hand, agreement with the experimentally measured[3] phonons is not especially good, the main failure of the simulation being the overestimation of the frequencies of the LO phonons. This is a straightforward consequence of the neglect of ionic polarization in our model, as we shall show in Sec. IV F. It should be noted that our use of a finite system means that we are unable to observe the $q = 0$ LO phonon.

At sufficiently low temperatures the phonons are all very well defined, the only feature of the spectrum being a sharp peak close to the quasiharmonic frequency. With increasing temperature the phonons shift and broaden, a behavior illustrated in Figs. 2 and 3 for selected longitudinal phonons propagating in the ⟨100⟩ direction. Figure 2 shows the neutron cross section for the zone-boundary LA phonon at the lowest and highest temperatures studied. The observed frequency shift is large, approximately 20%, but is nonetheless considerably smaller than that predicted by quasiharmonic theory. The other obvious effect of increasing the temperature is the growth in intensity at low frequencies. Figure 3 shows the neutron

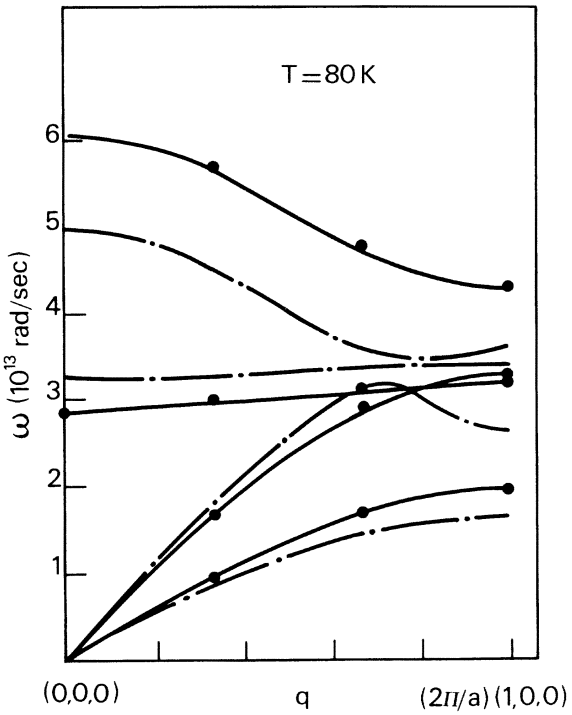

FIG. 1. Phonon frequencies for the ⟨100⟩ direction at 80 K. The dots are molecular-dynamics results and the solid lines give the quasiharmonic results for the same model. The dash-dot lines represent experimental neutron scattering data (Ref. 3).

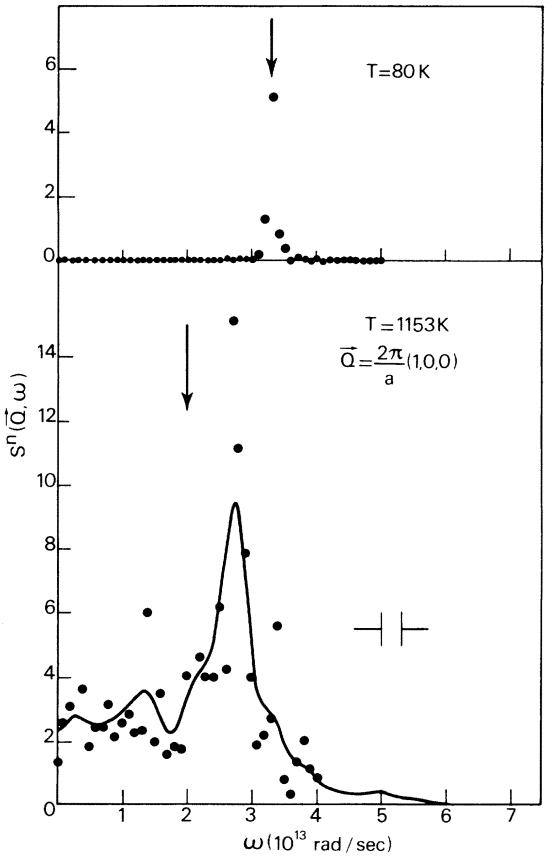

FIG. 2. Zone-boundary LA phonon (in arbitrary units) at two temperatures. The dots are molecular dynamics results and the arrows mark the location of the quasiharmonic frequencies. The curve represents the results of the smoothing procedure described in the text.

cross section at 302 and 1153 K for the smallest wave vector we can study in our periodic system of 216 ions, i.e., $\vec{Q} = (2\pi/3a)(1, 0, 0)$. The main peak is the LA phonon. This remains well defined as the temperature increases, and simultaneously a peak centered at $\omega = 0$ develops, so that the spectrum qualitatively resembles a Rayleigh-Brillouin triplet. The weak response at high frequency is shown in the inset diagrams; the peak near 5×10^{13} rad sec^{-1} corresponds to the LO mode. The dashed curves in the insets show the charge-weighted spectra, plotted on a different relative scale; this comparison between $S^n(\vec{Q}, \omega)$ and $S^z(\vec{Q}, \omega)$ aids the identification of the optic-mode frequency at high temperatures. As is well known, the relative intensity of the acoustic and optic peaks for the same $\vec{q}$ can be very different in different Brillouin zones, and this behavior can also be exploited in identifying a mode frequency.

In Fig. 3(a) the dots on the figure are the direct output from the molecular-dynamics calculations. At 954 and 1153 K the direct output is somewhat noisy, particularly at large momentum transfer, because our method of computing $S(\vec{Q}, \omega)$ necessarily includes the long-time statistical errors in $S(\vec{Q}, t)$. The noise level can be reduced by convoluting the calculated spectrum with a Gaussian filter of given width, say δ. This in turn is equivalent to truncating correlations in $\rho_{\vec{Q}}(t)$ beyond a time $\tau \simeq 2/\delta$. The solid lines in Figs. 2 and 3 show results obtained by this procedure; the width used for the filter is shown on each graph and is usually equivalent to 600 time steps. The correctness of the method can be checked by transforming the raw $S(\vec{Q}, \omega)$ data to yield $S(\vec{Q}, t)$, truncating the long-time tail at the appropriate value of τ, and the transforming back to obtain the smoothed $S(\vec{Q}, \omega)$.

C. TO ($q = 0$) phonon

The $q = 0$ TO phonon is of particular interest because it can be studied by infrared spectroscopic methods as well as in neutron scattering experiments. For this reason it is the only phonon on which experimental data are available at relatively high temperatures (up to approximately 700 K). In our calculations we have studied this particular

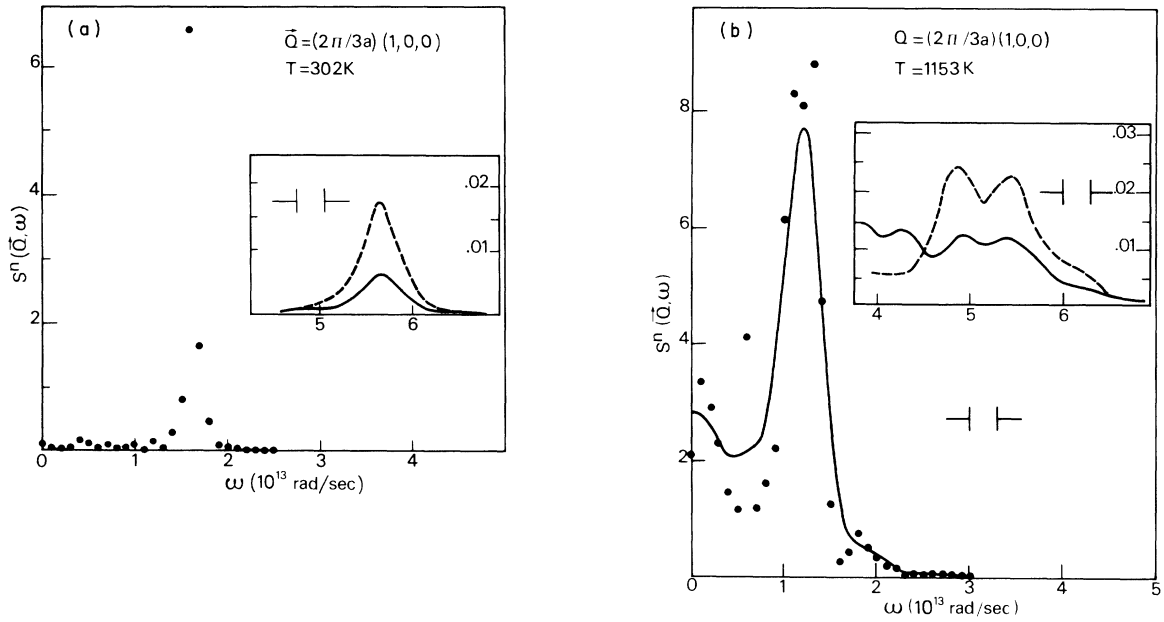

FIG. 3. (a) Neutron cross-section (in arbitrary units) for the smallest accessible wave vector. The curves in the inset show the high-frequency response in $S^n(\vec{Q},\omega)$, plotted on the same relative scale (full line), and in $S^z(\vec{Q},\omega)$, plotted on an arbitrary relative scale (dash line). (b) As (a) but at a higher temperature. The full curve in the main figure shows the effect of smoothing the molecular dynamics results.

phonon for a momentum transfer corresponding to $\vec{Q}=(2\pi/3a)(3,3,3)$ at temperatures of 302, 954, and 1153 K. At the lowest temperature the spectrum is sharp, as for all the phonons we have measured. At 954 K the peak is still clearly defined but sits now on a broad background. There is also some evidence for a weak secondary peak at approximately one-half the frequency of the main peak. At 1153 K the subsidiary peak has grown somewhat in intensity and a further satellite line can be seen at $\frac{3}{2}$ the main peak frequency. It is possible, of course, that the detailed structure of the spectrum is related to the small size of our system, but it could also represent a contribution from real multiphonon effects. The frequencies of the main peaks and their approximate full widths at half maximum height (with due allowance made for our resolution) are compared with experimental infrared results[16] in Fig. 4. The absolute values of the frequencies are too low, but the temperature dependence and the width are both in fairly good accord with the experimental data. The low value of the TO frequency reflects the inadequacy of the force constants in the Tosi-Fumi model, the question of polarization being of much less importance for this mode.

D. $\vec{Q}$ dependence and the one-phonon approximation

One of the original aims of this work was to investigate the $\vec{Q}$ dependence of the phonon spectra in an attempt to isolate the contribution from multiphonon processes. In Fig. 5 we show the charge-weighted spectrum $S^z(\vec{Q},\omega)$ and its one-phonon approximation $S_1^z(\vec{Q},\omega)$ for the LO phonon $\vec{Q}=(2\pi/3a)\times(7,0,0)$ at 302 K. In the one-phonon approximation the peak is asymmetric, whereas the full $S^z(\vec{Q},\omega)$ is essentially symmetric. The influence of the interference term in the phonon expansion (18) is clearly visible, even at this low temperature and low value of $\vec{Q}$. The interference effect in lowest order contributes a term proportional to Q^3 which changes sign as the phonon wave vector $\vec{q}$ $(=\vec{Q}\pm\vec{g})$ crosses a Bragg vector $\vec{g}$. In the case illustrated, the result is to move intensity from the left-hand side to the right-hand side of the peak, incidentally making the peak more symmetric. At higher temperatures the effect is even more marked, as Fig. 6 shows. The one-phonon approximation for $\vec{Q}=(2\pi/3a)(7,0,0)$ is virtually identical with the full result for $\vec{Q}=(2\pi/3a)(1,0,0)$ when due allowance is made for the factor $[Qd(Q)]^2$. Thus Figs. 5 and 6 display directly the $\vec{Q}$ dependence of this particular phonon. We see that at 954 K the center of gravity of the spectrum is noticeably shifted by the interference effect. The increase in temperature has led to a substantial growth in the multiphonon background, but the peak remains easily identifiable.

In the left-hand part of Fig. 6 we show the $\vec{Q}$ dependence of the corresponding LA phonon at 954 K.

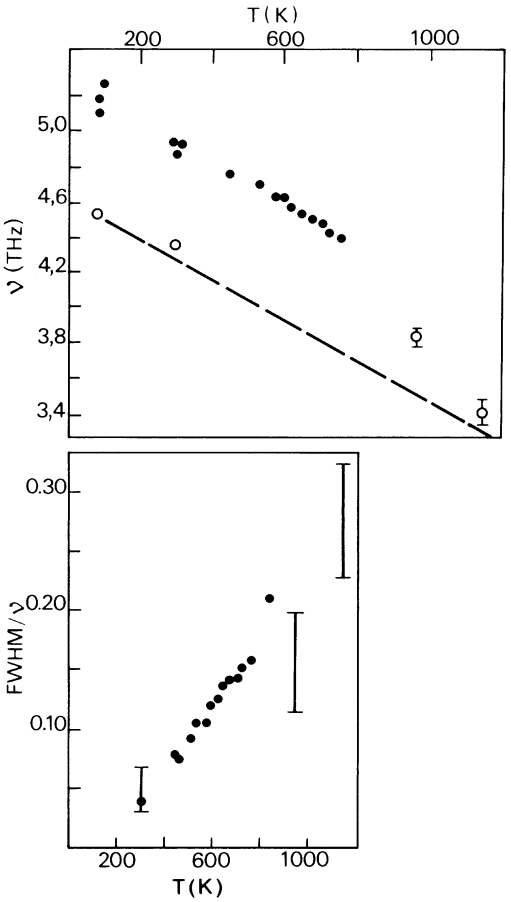

FIG. 4. $q=0$ TO mode. The upper half shows the peak frequency ν as function of temperature; circles are molecular-dynamics results, dots are experimental data (Ref. 15), and the dash line gives the predictions of quasiharmonic theory. The lower half shows the full width at half-maximum relative to ν; molecular-dynamics results are shown as error bars.

There is almost no evidence here of any interference effect, but the increase in the multiphonon background for $\vec{Q}=(2\pi/3a)(7,0,0)$ has caused a shoulder to appear on the side of the main peak. The one-phonon approximation has a peak at $\omega=0$, which is little different from that occurring in the full $S(\vec{Q},\omega)$ for the point $\vec{Q}=(2\pi/3a)(1,0,0)$ (shown as open circles). Thus the central peak is clearly not the result of multiphonon processes, lending support to our earlier suggestion that it is the remnant of a Rayleigh-type line.

Figures 7(a) and 7(b) show some of the phonons studied by Cowley and Buyers in their classic work[12] on the interference effect in KBr. To illustrate the importance of the effect we have plotted the neutron cross section $S^n(\vec{Q},\omega)$ and its one-phonon approximation for values of $\vec{Q}$ on either side of the Bragg vectors $\vec{g}=(2\pi/3a)(3,3,3)$ and $\vec{g}=(2\pi/3a)(9,9,9)$. For the smaller Bragg vector,

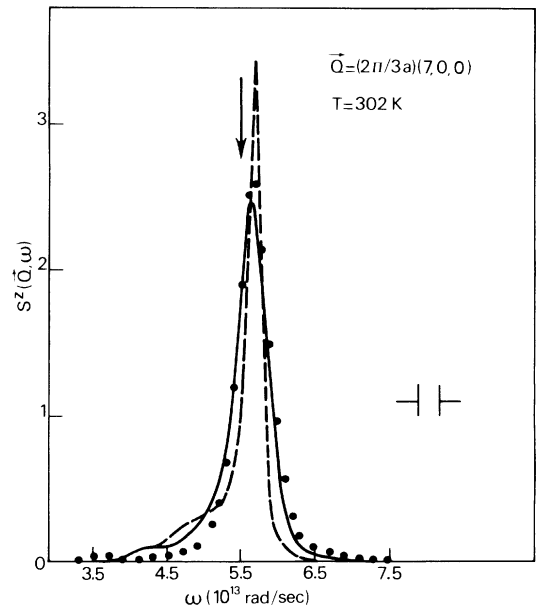

FIG. 5. Charge-weighted spectrum (in arbitrary units) for $\vec{Q}=(2\pi/3a)(7,0,0)$ at 302 K. The dots are the molecular-dynamics results for $S^z(\vec{Q},\omega)$ and the line shows the corresponding one-phonon approximation. The dashed line gives the results for $S_1^z(\vec{Q},\omega)$ from perturbation theory and the arrow locates the quasiharmonic frequency.

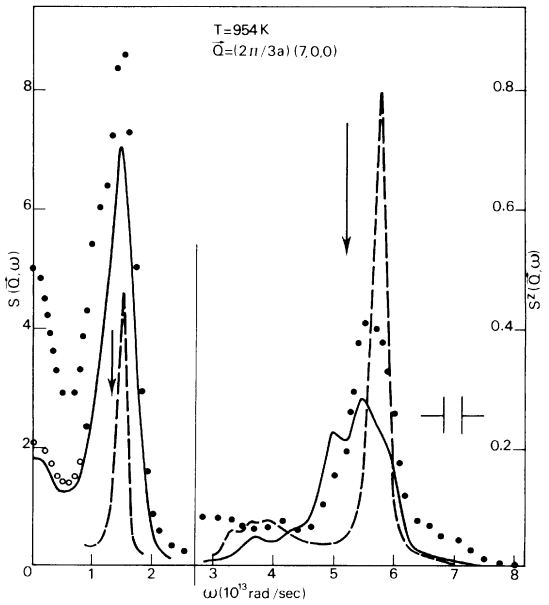

FIG. 6. Right-hand part same as in Fig. 5, but at a higher temperature. The left-hand part shows $S(\vec{Q},\omega)$ for the same wave vector $[\vec{Q}=(2\pi/3a)(7,0,0)]$. Results for $\vec{Q}=(2\pi/3a)(1,0,0)$, scaled by the factor $[Qd(Q)]^2$, are shown as open circles. For the sake of clarity, the perturbation results have been reduced in intensity by a factor of 4.

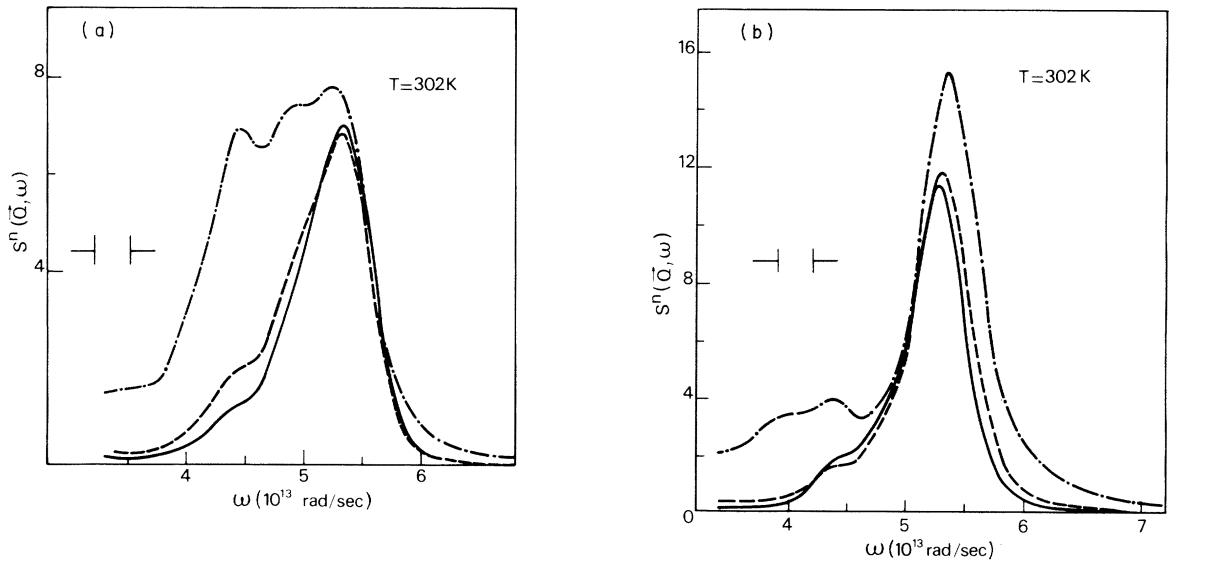

FIG. 7. (a) The interference effect in the neutron cross section at 302 K. The full curve is $S_1^n(\vec{Q},\omega)$ and the broken curves are $S^n(\vec{Q},\omega)$ for $\vec{Q}=(2\pi/3a)(2,2,2)$ (dashes) and $\vec{Q}=(2\pi/3a)(8,8,8)$ (dash-dot). The spectra have in all cases been divided by $[Qd(Q)]^2$. (b) As (a) but for wave vectors $\vec{Q}=(2\pi/3a)(4,4,4)$ (dashes) and $\vec{Q}=(2\pi/3a)(10,10,10)$ (dash-dot).

where the spectra are not complicated by multiphonon effects, the interference effect is clearly visible. For the larger one, both the multiphonon and interference effects have grown in magnitude and are not so readily separable. However, there is clearly a large enhancement of intensity on the low-frequency side of the spectrum for $\vec{Q}=(2\pi/3a)\times(8,8,8)$ and on the high-frequency side for $\vec{Q}=(2\pi/3a)(10,10,10)$. The relative effects seen here are not symmetrical. This arises from the necessity of both spectra (when divided by Q^2) having the same second moment; clearly the transfer of intensity from high to low frequency must be accompanied by a correspondingly greater enhancement of the spectrum relative to $S_1^n(\vec{Q},\omega)$ than in the reverse case.

E. Comparison with perturbation theory

Figures 5 and 6 show a comparison between the molecular-dynamics results for $S_1^s(\vec{Q},\omega)$ at the smallest accessible wave vector, i.e., $\vec{Q}=(2\pi/3a)\times(1,0,0)$, and the predictions of anharmonic perturbation theory. At 302 K (Fig. 5) there is reasonably good agreement. Both calculations give rise to a peak which is asymmetric (in the same sense) and shifted to a frequency higher than the quasiharmonic result. (Note that both spectra have been convoluted with the same smoothing function.) The simulation gives a broader peak and the shift from the quasiharmonic frequency is somewhat smaller. However, the perturbation theory used here is limited by the assumption that one phonon decays into two others, and therefore yields a lower limit on the width of the phonon or, equally, an upper limit on the lifetime.

At 954 K (Fig. 6) the molecular dynamics result for the same phonon is much broader and shifted noticeably less from the quasiharmonic frequency than in the perturbation calculations. In the case of the wave vector $\vec{Q}=(2\pi/3a)(7,0,0)$ there is somewhat better agreement with the full $S^s(\vec{Q},\omega)$ than with the one-phonon approximation. This, of course, is fortuitous, because the full result in-

TABLE III. Phonon frequencies, in units of 10^{13} rad sec^{-1} for $(\vec{Q})=(2\pi/3a)(3,0,0)$.

T (K)		TA	LA	TO	LO
80.3	QH	1.93	3.28	3.14	4.28
	APT	1.92	3.29	3.15	4.26
	MD [a]	1.90	3.30	3.15	4.30
301.7	QH	1.92	3.08	2.94	4.23
	APT	1.89	3.16	3.02	4.18
	MD	1.90	3.15	3.00	4.20
500.0	QH	1.92	2.91	2.78	4.19
	APT	1.85	3.05	2.91	4.14
700.0	QH	1.90	2.73	2.62	4.15
	APT	1.83	2.98	2.81	4.09
953.8	QH	1.89	2.54	2.45	4.11
	APT	1.82	2.9 [b]	2.70	4.04
	MD	1.75	2.85	2.75	4.05

[a] MD, molecular-dynamics results, with typical statistical uncertainty of ± 0.05.

[b] Very broad.

cludes a significant contribution from the interference effect. It is possible to extend the perturbation calculations to take account of the interference term, but we have not so far attempted this. The satellite peak in the molecular dynamics result is less separated from the main peak than in the perturbation calculation. Qualitatively this can be understood as resulting from the neglect of phonon renormalization in the basis set used in the perturbation theory. In the simulation, the phonon linewidth arises from interactions between phonons which already have a finite width and shift compared with the harmonic approximation. Hence any fine structure in the phonon spectral function will necessarily be shifted (relative to the main peak) and broadened when compared with that found in a simple perturbation calculation.

In Table III we make detailed comparison between the molecular-dynamics results and the theoretical predictions for the frequencies of the zone-boundary ⟨100⟩ phonons. Since zone-boundary phonons display no interference effect, the comparison is a meaningful one, even though the perturbation calculation of the neutron cross section is limited to the one-phonon approximation. For this particular value of $\vec{Q}$, the TA and LO phonons show only small negative shifts from the quasiharmonic results, whereas the LA and TO shifts are large and positive. (The shift in the LA phonon and its temperature dependence are also illustrated in Fig. 2.) Such a variety of behavior clearly constitutes a severe test of a theory of anharmonic effects. In fact, as the table shows, agreement between the molecular-dynamics and perturbation theory calculations is excellent at 302 K and remains good even at 954 K. Thereafter the perturbation theory rapidly breaks down and no useful comparison can be made at 1153 K. Nonetheless, at least insofar as the prediction of the phonon frequencies are concerned, the perturbation method used here remains adequate up to temperatures roughly 80% of melting. The range of validity of the theory is therefore substantially greater than in comparable calculations on rare-gas solids.[17]

F. Effect of ionic polarization

As we have already stressed, the Tosi-Fumi model takes no account of ionic polarization and for that reason is unable to account quantitatively for details of the dynamical properties of NaCl. The effect of polarization on the interionic forces can be incorporated explicitly in a molecular-dynamics simulation, though at the cost of a considerable increase in computing time. The technical problems involved in such a calculation have been discussed in detail in a recent paper,[18] both for a model consisting of point polarizable ions and for a simple version of the shell model. In the shell model the total ionic charge is assumed to be divided between a core and a shell, and polarization corresponds to a bodily displacement of the shell with respect to the core. The shell, which represents the outer electron cloud, is assumed to be bound to the core by a harmonic potential and the short-range repulsive interactions are assumed to act between the shells. In the molecular-dynamics "experiment" the equations of motion of the cores are solved in the usual way, whereas the shells are assumed to adjust themselves instantaneously so as to minimize the total potential energy of the system. The second step is considerably more complicated to carry out than the first and requires the use of iterative methods. Use of the shell model in molecular-dynamics calculations has also been discussed by Dixon and Sangster.[19]

In Fig. 8 we show a typical result obtained from a shell-model calculation in which polarization is superimposed on the Tosi-Fumi potential for NaCl. Only the Cl^- is treated as polarizable, the parameters of the model (the charge on the shell and the spring constant in the shell-core potential) being taken from the work of Sangster.[20] The phonon shown corresponds to the LO mode of smallest wave vector. There is a large negative shift with respect to the rigid-ion result, bringing the phonon frequency into good agreement with the experimental value (see Fig. 1). Such effects are, of course, already well known from lattice-dynam-

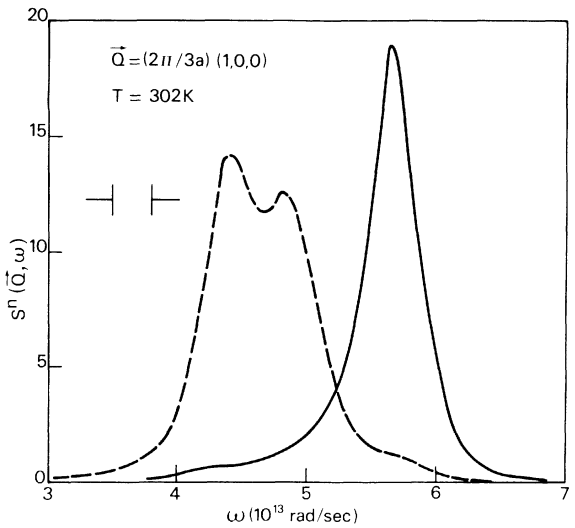

FIG. 8. Effect of polarization on the charge-weighted spectrum (in arbitrary units) for $\vec{Q} = (2\pi/3a)(1, 0, 0)$ at 302 K. The full curve shows results from the rigid ion "experiment," the dash curve those from a shell-model simulation.

ical calculations; we include the comparison here primarily to demonstrate that the molecular-dynamics simulation can be made substantially more realistic if this is particularly required. The broadening of the spectrum and the appearance of a double-peaked response is qualitatively similar to the behavior found by Cowley[10] in a perturbation calculation for the $q=0$ LO mode. Since polarization acts in such a way as to reduce the phonon frequencies (though the effect in other branches is less pronounced than for the LO mode), its inclusion necessarily leads to an increase in the amplitudes of vibration. This effect turns out to be very large, as shown by the results given in Table IV.

TABLE IV. Root-mean-square displacements of the ions. d ($=\frac{1}{2}a$) is the nearest-neighbor separation.

T (K)	$100\langle u_+^2\rangle^{1/2}/d$ MD [a]	QH	$100\langle u_-^2\rangle^{1/2}/d$ MD	QH
(i) Rigid ions				
80.3	4.5	4.0	4.0	3.8
301.7	8.2	7.8	8.0	7.6
953.8	17.0	15.4	15.8	14.8
1153.0	20.6	19.0	19.5	18.5
(ii) Polarizable ions [b]				
306.3	12.6		11.0	
1153.5	24.3		23.6	

[a] MD, molecular-dynamics results.
[b] Shell-model results from Ref. 18.

V. CONCLUSIONS

The results reported here demonstrate that computer simulation can play a valuable role in analyzing the lattice vibrations of a simple ionic crystal such as NaCl. The fact that the one-phonon approximation to the dynamic structure factor can be evaluated in parallel with the calculation of the complete spectrum means that anharmonic effects can readily be isolated and their importance assessed. Our main quantitative result is that a simple perturbation treatment is adequate for the prediction of phonon frequencies at temperatures up to 80% of the melting temperature; on the other hand, the phonon linewidths are underestimated, particularly at high temperatures. In making this comparison it is sufficient to work with a much oversimplified potential model and most of our calculations have, in fact, been made for a system of rigid ions. The effects of polarization can be included, however, though only at considerable added expense in computing time, and fair agreement with experimental results can then be achieved. However, the qualitative features of our results are likely to be insensitive to details of the interionic potential, and hence should carry over to other ionic systems.

ACKNOWLEDGMENTS

We are grateful to C. Moser for providing the computing time which made the molecular-dynamics calculations possible. The work has been supported, in part, by a grant from the United Kingdom Science Research Council.

*Permanent address: G.N.S.M., Consiglio Nazionale delle Richerche, Instituto di Fisica, Università di Roma, Roma, Italy.
†Permanent address: Chemistry Division, National Research Council of Canada, Ottawa K1A 0R6, Canada.

[1] E. W. Kellermann, Philos. Trans. R. Soc. Lond. 238, 63 (1940).
[2] (a) F. G. Fumi and M. P. Tosi, J. Phys. Chem. Solids 25, 31 (1964); (b) M. P. Tosi and F. G. Fumi, *ibid.* 25, 45 (1964).
[3] G. Raunio, L. Almqvist, and R. Stedman, Phys. Rev. 178, 1496 (1969).
[4] B. G. Dick and A. W. Overhauser, Phys. Rev. 112, 90 (1958).
[5] J. R. Hardy, Philos. Mag. 7, 315 (1962).
[6] U. Schröder, Solid State Commun. 4, 347 (1966).
[7] D. J. Adams and I. R. McDonald, J. Phys. C 7, 2761 (1974); 8, 2198 (1975).
[8] (a) R. A. Cowley, Adv. Phys. 12, 421 (1963); (b) R. A. Cowley, Rep. Prog. Phys. 31, 123 (1968).
[9] E. R. Cowley, J. Phys. C 4, 988 (1971).
[10] E. R. Cowley, J. Phys. C 5, 1345 (1972).
[11] H. R. Glyde and M. L. Klein, Crit. Rev. Solid State Sci. 2, 181 (1971).
[12] (a) R. A. Cowley and W. J. L. Buyers, J. Phys. C 2, 2262 (1969); (b) R. A. Cowley, E. C. Svensson, and W. J. L. Buyers, Phys. Rev. Lett. 23, 525 (1969).
[13] H. Horner, Phys. Rev. Lett. 29, 556 (1972).
[14] D. Levesque, L. Verlet, and J. Kürkijarvi, Phys. Rev. A 7, 1690 (1973).
[15] V. Ambegoakar, J. Conway, and G. Baym, in *Lattice Dynamics*, edited by R. F. Wallis (Pergamon, New York, 1965), p. 261.
[16] J. E. Mooij, W. B. Van de Bunt, and J. E. Schrijvers, Phys. Lett. A 28, 573 (1969).
[17] J. P. Hansen and M. L. Klein, Phys. Rev. B 13, 878 (1976).
[18] G. Jacucci, I. R. McDonald, and A. Rahman, Phys. Rev. A 13, 1581 (1976).
[19] M. Dixon and M. J. L. Sangster, J. Phys. C 8, L8 (1975); 9, L5 (1976).
[20] M. J. L. Sangster, J. Phys. Chem. Solids 34, 355 (1973).